Applied Catalysis B: Environmental 174–175 (2015) 21–34

Contents lists available at ScienceDirect

Applied Catalysis B: Environmental

journal homepage: www.elsevier.com/locate/apcatb

A study of Ni/Al_2O_3 and $Ni–La/Al_2O_3$ catalysts for the steam reforming of ethanol and phenol

Gabriella Garbarino[a,b], Chongyang Wang[b], Ioannis Valsamakis[b], Sahar Chitsazan[a], Paola Riani[c], Elisabetta Finocchio[a], Maria Flytzani-Stephanopoulos[b], Guido Busca[a,*]

[a] Università degli Studi di Genova, Dipartimento di Ingegneria Civile, Chimica e Ambientale (DICCA), Laboratorio di chimica delle superfici e catalisi, P.zzale Kennedy, 1 16129 Genova, Italy
[b] Department of Chemical and Biological Engineering, Tufts University, Medford, MA, USA
[c] Università degli Studi di Genova, Dipartimento di Chimica e Chimica Industriale (DCCI), Via Dodecaneso, 31 16146 Genova, Italy

ARTICLE INFO

Article history:
Received 18 December 2014
Received in revised form 11 February 2015
Accepted 20 February 2015
Available online 23 February 2015

Keywords:
Nickel catalysts
Lanthana on alumina
Alumina-supported catalysts
Phenol steam reforming
Ethanol steam reforming
Tars steam reforming
Sulfur deactivation

ABSTRACT

$La_2O_3/\gamma–Al_2O_3$, $NiO/\gamma–Al_2O_3$ and $NiO/La_2O_3/\gamma–Al_2O_3$ samples have been prepared by conventional impregnation, using silica-free γ-Al_2O_3 support. The materials have been characterized, as such or after reaction, with XRD, skeletal IR, UV–vis–NIR, XPS and FESEM techniques. The catalytic activity has been evaluated in ethanol decomposition through temperature programmed surface reaction (TPSR); and in ethanol steam reforming (ESR); and in mixed ethanol and phenol steam reforming (EPSR as a model reaction for biomass tar steam reforming) in a continuous flow reactor. Ni on alumina exists as a surface $Ni_xAl_2O_{3+x}$ spinel, evident by XRD, skeletal IR and vis spectroscopy measurements. La disperses on alumina in a disordered state. In the ternary system, XPS reveals significant Ni–La interactions. The addition of some lanthanum further increases the activity of Ni/Al_2O_3 for ESR and EPSR. Fresh unreduced catalysts are conditioned in the feed at temperatures above 973 K. Conditioned catalysts give rise to full conversion of reactants in ESR and EPSR at 873 K and higher temperatures, but are severely deactivated by sulfur. The sudden start of the steam reforming activity at 873 K likely corresponds to the temperature onset for the activation of water by metallic nickel.

1. Introduction

Supported Ni catalysts are widely used for the steam reforming of methane and natural gas [1,2]. This process, performed at 973–1173 K, is the most applied for the production of hydrogen and syngas today. The wide application of these catalytic materials demonstrates their efficiency as well as reliability. For stable operation, however, feed gas pre-treatment is needed such as desulphurization and pre-reforming of higher hydrocarbons, in order to avoid catalyst deactivation by sulfur poisoning as well as the formation of carbonaceous matter. Due to the high reaction temperature (>1073 K), the support must be a stable refractory material, such as α-A_2O_3 (corundum), or Mg or Ca aluminates.

Similar-type catalysts are applied at lower temperatures for pre-reforming of propane and butane (773–873 K) [1–3] and as catalysts for a number of hydrogenation reactions (473–673 K) [4,5]. Working at these lower temperatures, transitional aluminas may be stabilized by alkali, alkaline earth, rare earths or silica [6]. These catalyst compositions have been found promising in experimental studies aimed at the development of efficient catalysts for ethanol steam reforming (ESR [7,8]), biomass tar steam reforming [9,10] and bio-oil steam reforming [8,11], all processes allowing, in principle, the production of hydrogen and syngas from renewable matter and working in the 773–973 K temperature range. In previous studies, it was found that Ni/Al_2O_3 catalysts are very active in the steam reforming of ethanol and phenol (EPSR), whose mixture is taken as a model of biomass tar mixture, but they deactivate in the presence of sulfur in the feed [12]. The addition of Mg and B has also been investigated: Mg further increases the catalytic activity but does not improve the sulfur resistance, while B deactivates the catalyst but may have a slight beneficial effect on sulfur resistance [13]. These studies were performed using an alumina support stabilized by small amounts of silica.

The addition of La is known to stabilize alumina for high temperature applications [14] and was also found to improve the resistance to coking of Ni/Al_2O_3 catalysts in steam reforming of propane [15] and of ethanol [16] and in dry reforming catalysis [17]. Lanthanum oxide was also found to improve the activity of

* Corresponding author. Tel.: +39 103536024; fax: +39 103536028.
E-mail address: Guido.Busca@unige.it (G. Busca).

http://dx.doi.org/10.1016/j.apcatb.2015.02.024
0926-3373/

Table 1
Composition, surface area and hydrogen consumption data.

	NiO loading	La_2O_3 loading	BET Surface area	H_2 consumption	H_2/Ni
	$w_{NiO}/w_{support}$ (%)	w_{La2O3}/w_{Al2O3} (%)	(m^2/g)	(μmol/g)	
A	–	0	170	n.a.	n.a.
LA	–	20%	151	n.a.	n.a.
NiA	20%	0	148	3159	1.18
NiLA	20%	20%	131	3051	1.14

low-temperature Rh-based catalysts in phenol steam reforming [18]. Additionally, it has been reported that lanthana can be used as precursor of sulfur-tolerant water-gas shift catalysts, being converted in situ to lanthanum oxysulfide (La_2O_2S) [19]. Thus, it was of interest to test whether the addition of lanthanum can provide improved activity and some sulfur stability to the catalyst. To investigate the potential improvement of activity and stability of Ni/Al_2O_3 based catalysts for tar and ethanol steam reforming we compared pure alumina and alumina stabilized by lanthana as catalyst supports.

2. Experimental

2.1. Materials preparation

The catalyst were prepared using Puralox 200 Sba (γ-Al_2O_3, 200 m^2/g) from Sasol previously calcined at 1023 K for 5 h as bare support. The catalytic materials, summarized in Table 1, were prepared through incipient wetness impregnation using $La(NO_3)_3{\cdot}xH_2O$ ($x \sim 4$) and $Ni(NO_3)_2{\cdot}6H_2O$ (from Alfa Aesar and Sigma–Aldrich, respectively) aqueous solutions. The theoretical amounts of La and Ni to obtain 20% oxide on alumina (measured as 100 g_{MO}/100 g_{supp} where MO is La_2O_3 or NiO and supp is either Al_2O_3 (A) or 20%La_2O_3/Al_2O_3 (LA)) was dissolved in a volume of deionised water in the way that the total liquid volume was equal to the pore volume of the material. A step of drying at 353 K in vacuum was undertaken for 15 h and calcination in air at 1023 K for 5 h was performed. The NiLA catalyst was prepared using LA as the support, thus the first impregnation was with La and the second with Ni precursors.

2.2. Materials characterization

Surface area measurement was done in a Micromeritcs Autochem 2920 with a single point measurement. The samples were pretreated in He at 523 K in order to desorb or decompose potentially adsorbed surface species.

X-Ray diffraction patterns were recorded using Cu Kα radiation (λ = 0.15406 nm). XRD analysis of the fresh catalysts was performed on a Rigaku Smartlab Cu-source powder diffractometer. Cu Kα radiation was used with a power setting of 45 kV and 200 mA. Scan rate of 2°/min with a 0.02° step size was used; while those of exhaust samples were obtained using a vertical powder diffractometer X'Pert. The patterns were collected in the 25–100° 2θ range with a step of 0.03° and a counting time for each step of 12 s. Powder patterns were indexed by comparing experimental results to the data reported in the Pearson's crystal data database [20].

Temperature programmed reduction (TPR) tests were used to identify and evaluate the reducibility of the various nickel species present on the alumina-supported catalysts. In a typical H_2-TPR test the as-calcined catalyst was reduced by a 10% H_2/Ar gas mixture, while the temperature was increased from RT to 1173 K at a rate of 15 K/min. In Table 1 the mol_{H2}/mol_{Ni} hydrogen consumption data during TPR are reported.

FT IR studies were performed on compacted powder disks of 20–30 mg activated in vacuum at 773 K before adsorption experiments. CO_2 (several Torr) was adsorbed at room temperature and spectra were recorded in the presence of the gas and after outgassing at room temperature and at increasing temperature. A Nexus ThermoNicolet instrument was used (OMNIC software, DTGS detector, 100 scans). All the spectra are reported in common scale.

X-ray photoelectron spectroscopy (XPS) was conducted by using the Thermo Scientific monochromatic Al K-alpha line (1.4866 keV) as the excitation source. Binding energies were measured on a multi-channel detector with pass energy of 50 eV and energy step of 0.05 eV for high resolution scans and 0.5 eV for survey scans. Spectral regions are Ni2p, Al2p and La3d. All the spectra were referenced to the elemental carbon at binding energy (BE) of 284.8 eV. Quantification of surface components was based on the peak fitting and normalization of Ni (2p3/2), La (3d5/2), and Al (2p) primary peaks.

Microscopic analyses were performed on a SEM ZEISS SUPRA 40 VP microscope, equipped with a field emission gun. This instrument is equipped with a high sensitivity "InLens" secondary electron detector and with a EDX microanalysis OXFORD "INCA Energie 450 × 3". Samples for SEM analysis were suspended in ethanol under ultrasonic vibrations to decrease particle aggregation. A drop of the resultant mixture was deposited on a Lacey Carbon copper grid and the dried sample was then imaged.

2.3. Catalytic experiments

Temperature programed surface reaction (TPSR) dynamic experiments with ethanol were done with 0.1 g of catalysts diluted in 0.2 g quartz beads by varying the temperature from RT to 973 K in 4 h and holding at that temperature for 10 min. The flowrate was set at 50 ml/min and the ethanol concentration was 7.9% (% v/v) fed with a syringe pump. The analysis of the product gas was done with a mass spectrometer following sixteen different m/z values; and to obtain a quantitative measurement, a three point calibration was done for each evolved species. Moreover, a complete analysis was done in order to separate the overlap between signals, thus obtaining quantitative results (mol/mol, %).

A tubular quartz flow reactor, containing a fixed bed with 44.1 mg of catalyst mixed with 440 mg of quartz particles 0.25–0.21 mm (corresponding to 60–70 mesh sieved) was used in steady-state catalytic experiments. For the experiments concerning ethanol conversion in the presence of steam the feed gas was composed of a mixture of ethanol and water with a molar ratio (water to ethanol) equal to 6 in He (41.6% v/v) added as carrier gas. The gas hourly space velocity GHSV was equal to 51,700 h^{-1} (NTP). In order to follow any hysteresis or deactivation effects, experiments were performed both in ascending and descending reaction temperature (523 K, 673 K, 773 K, 873 K, 973 K, 1023 K and reverse).

For testing the tar model mixture, 40 Nml/min (GHSV = 54000 h^{-1}) of a gaseous mixture with the following composition: 39.3% He, 54.6% water, 4.1% ethanol and 2% phenol; was used. A phenol–water–ethanol single phase liquid solution was pumped through a HPLC pump (Shimadzu Corp., LC-D10 AD) in an appropriate heating section at 583 K of the feed line to produce a gas mixture whose composition corresponds to 168 g/Nm^3 of ethanol + phenol (84.9 g/Nm^3 of phenol), and 439 g/Nm^3 water vapor in the He inert carrier. No catalyst pretreatments were

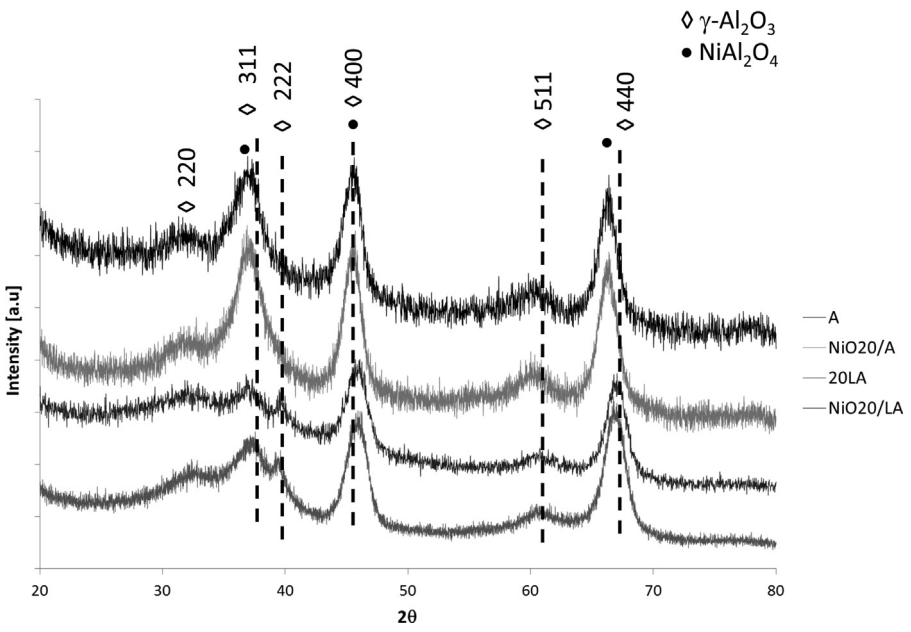

Fig. 1. XRD diffraction patterns of the materials under investigation (◊ γ-Al2O3 and • $NiAl_2O_4$).

performed. The reactor temperature was varied from 773 K to 1023 K, and vice–versa. The measured bed temperature was slightly lower than the furnace temperature according to the overall endothermicity of the involved reactions.

To investigate sulfur poisoning, tetrahydrothiophene (C_4H_8S, THT) was used as a contaminant of the feed, as in a previous report [21]. In this case a pre-conditioning of the catalyst at 1023 K for 30 min in the feed gas was undertaken in order to activate the catalyst. The experiment was performed at 973 K, the effects of two sequential pulses of THT (first 0.011 mol_S/mol_{Ni} and after 0.033 mol_S/mol_{Ni}) and of a further stay on the sulfur-free stream on the catalytic activity of Ni–La containing sample was studied. In this case the THT was pulsed by injecting, with a syringe, the corresponding quantity of liquid in the preheating zone.

Product analysis was performed with a gas-chromatograph Agilent 4890 equipped with a Varian capillary column "Molsieve 5 A/Porabond Q Tandem" and TCD and FID detectors in series. Between them a nickel catalyst tube was employed to reduce CO and CO_2 to CH_4. Products analysis was also performed with a GC/MS (ThermoFisher), in order to have a precise identification of the involved compounds.

$$X_{reactant} = \frac{n_{react.in} - n_{react.out}}{n_{react.in}} \quad (1)$$

while selectivity to product *i* is defined as follows:

$$S_i = \frac{n_i}{\nu_i(n_{react.in} - n_{react.out})} \quad (2)$$

where n_i is the moles number of compound *i*, and ν_i is the ratio of stoichiometric reaction coefficients. When applied to the overall carbon feed, n_i is the carbon moles number of compound *i*, n_{react} is the carbon moles number of reactants mixture as a whole and $\nu_i = 1$. Hydrogen yield was defined for ESR experiments as $n_{H2out}/(6 \times n_{ethanolin})$, while for tar SR experiments $mol_{H2out}/(6 \times n_{ethanolin} + 14 \times n_{phenolin})$.

3. Results

3.1. Characterization of the fresh catalyst

3.1.1. Surface area measurements

The surface area of the pure alumina support decreases upon calcination at 1023 K for 5 h from 200 m^2/g to 170 m^2/g. The surface area is further reduced after the procedure of lanthanum impregnation and calcination down to 151 m^2/g. Ni addition further reduces the surface area, almost by the same factor of La addition, giving a final surface area of 148 m^2/g for NiA and 131 m^2/g for NiLA.

3.1.2. XRD

In Fig. 1 the XRD patterns of the samples under study are reported. The XRD diffraction patterns of the LA and A support present the pattern of γ-alumina, assumed to be a nearly cubic non-stoichiometric spinel [22], although the peaks in the LA pattern are weaker than in the A pattern. On the other hand, peaks of crystalline lanthanum species cannot be observed in the LA pattern. The addition of nickel to the two supports gives rise to an intensification of the peaks assigned to the 400 and 440 spinel peaks and, in particular, to that assigned to the 311 peak, with almost the disappearance of the 222 peak. The resulting pattern looks identical to that of $NiAl_2O_4$ stoichiometric inverted spinel [23]. This can be taken as surprising being the virtual composition of our sample, assuming full diffusion of Ni into the spinel bulk, $Ni_{0.26}Al_2O_{3.26}$, is still cationically deficient with respect to the spinel stoichiometry. However, previous studies showed that cationically deficient Ni aluminates may have a similar XRD pattern to that of stoichiometric $NiAl_2O_4$ [23]. A further evidence of the strong interaction of Ni with alumina with the formation of bulk or subsurface Ni aluminate layers comes from the evident shifts of the peaks of spinel structure, such as the 440 peak. The shift downwards of the 2θ values of the peaks corresponds to the entrance of Ni into the oxide cubic close packed array which causes a light expansion of the volume of the cubic unit cell, as discussed elsewhere [24].

We note here that the situation with "pure" alumina and lanthana alumina is different from that we previously found with a silica-containing γ-alumina support having a similar surface area [25]: in that case we found that the addition of the same amount

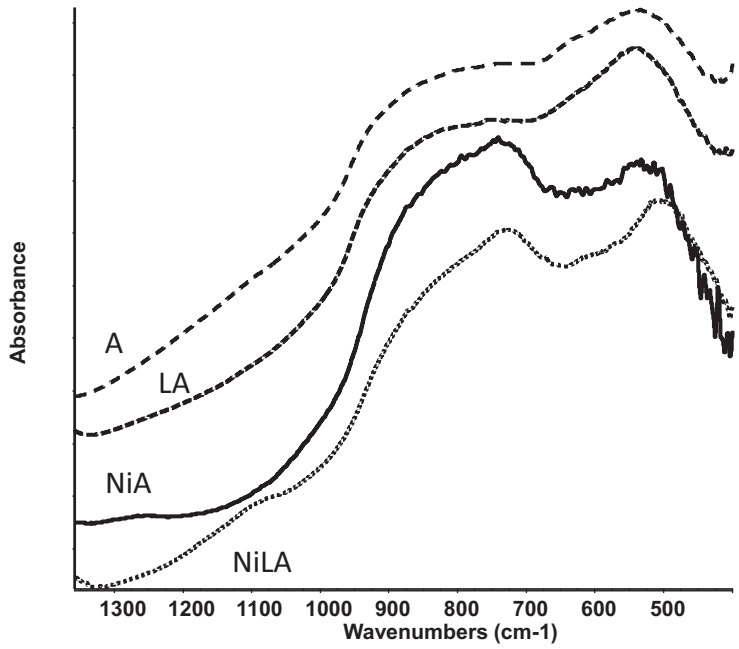

Fig. 2. Skeletal IR spectra of supports and Ni based materials.

of nickel leads to the appearance of the XRD peaks due to small amounts of NiO superimposed to the apparently non-perturbed peaks of γ-Al_2O_3. This suggests that small amounts of silica can prevent by strong interaction of Ni with alumina to Ni aluminate-like species, which is observed in the present case. Apparently, the addition of lanthanum, unlike silica, does not limit the Ni-alumina interaction as evidenced by the lack of unassociated NiO species.

3.1.3. Skeletal IR and UV–vis spectroscopic characterization

In Fig. 2the infrared skeletal spectra of the materials are reported. The alumina spectrum confirms the results obtained by XRD showing the typical features of γ-Al_2O_3 [22]. The same peaks were found on the lanthanum containing sample, thus confirming that the interaction of La species with the alumina bulk is small, if any, as also suggested by the XRD patterns. The presence of Ni changes significantly the shape of the curves with the appearance of a main band at 730 cm^{-1} and a pronounced feature at 505 cm^{-1}, with shoulders at 880, 790 and 600 cm^{-1}, thus giving rise to a spectrum very similar to that of powders of $NiAl_2O_4$ spinel, but also similar to that of cationically deficient $Ni_xAl_2O_{3+x}$ spinels [23]. Also IR spectra does reveal the presence neither of bulk NiO [26] nor of La- containing species.

The diffuse reflectance UV–visible and near infrared spectra (DR-UV–vis–NIR) of the catalysts are reported in Fig. 3. Both the pure alumina support and the LA sample do not show any evident absorption at the scale used in the figure. In contrast, both nickel containing samples spectra show absorptions in the visible region, i.e., a split band at 16,667 and 15,827 cm^{-1}, corresponding to λ = 600 and 633 nm, and a broad band in the NIR region, near 9090 cm^{-1} (1078 nm). The absorptions in the visible–NIR regions are associated to d → d transitions of Ni^{2+}, their shape and position being similar to those reported for $NiAl_2O_4$ [27] as well as for Ni highly dispersed on alumina [24,25].

The absorption in the UV region is typically associated with charge transfer transitions that gives rise in bulk oxides to bandgap transition. As it is well-known alumina is an insulator and its bandgap transition falls in the far-UV, i.e., at higher energy out of the range available with our instrument. A weak absorption observed in the spectrum of LA at 280 nm in the near-UV region is likely associated to O^{2-} (2p) → La^{3+} CT. In the spectra of both NiA and NiLA the absorption tail in the range 240–300 nm is likely the higher wavenumber side of an absorption associated to a O^{2-} (2p) → Ni^{2+} (3 d) CT. In any case the spectra observed for the NiA and NiLA catalysts are almost identical with each other and very similar to those reported previously and assigned to "isolated" Ni^{2+} species dispersed on alumina in an environment similar to that of $NiAl_2O_4$ spinel. These spectroscopic data indicate that, even in the presence of lanthanum, nickel strongly interacts with alumina.

3.1.4. Characterization of surface basicity by IR spectroscopy of adsorbed CO_2

Carbon dioxide is a good probe molecule for the characterization of surface basicity [28]. In Fig. 4 the IR spectra of the adsorbed species arising from the adsorption of CO_2 on A, LA and NiLA are compared. The bands at 1653 cm^{-1}, 1484 cm^{-1} (with 1453 cm^{-1} as a shoulder) and 1236 cm^{-1} are due to surface bicarbonate species (C═O asymmetric and symmetric stretching, and OH deformation, respectively [29]). These bands show that over hydroxylated alumina few nucleophilic (basic) hydroxyl- groups exist converting CO_2 into bicarbonate species. The spectra of adsorbed species are

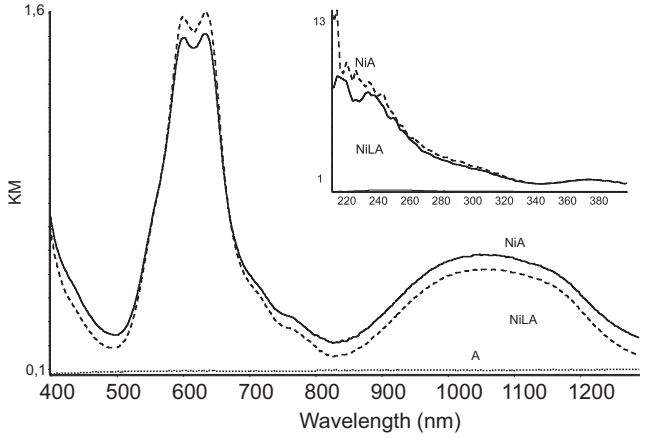

Fig. 3. DR-UV–vis–NIR spectra of the materials.

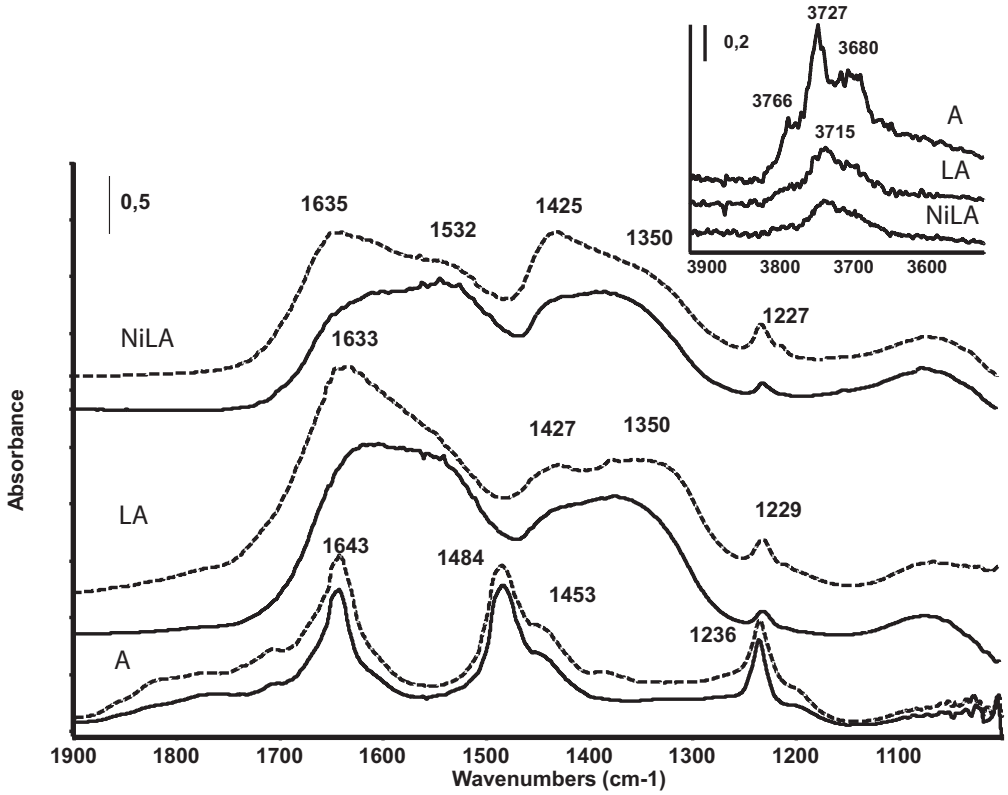

Fig. 4. FT-IR spectra of the adsorbed species arising from CO_2 adsorption on A, LA and NiLA: in contact with CO_2 gas (dash lines) and outgassed at room temperature (straight line). In the inset: IR spectra (νOH) of hydroxyl groups after activation at 773 K in vacuum for the three samples.

definitely modified after La addition. In this case the bands due to bicarbonate species definitely disappear while bands due to two types of carbonate species (couples at ca. 1635 and 1350 cm^{-1}, and at ca 1530 and 1425 cm^{-1}, asymmetric and symmetric C=O stretching) are formed. This shows that La addition provides new basic and nucleophilic sites for CO_2 adsorption. The further addition of Ni does not change the spectra. The spectra of the surface hydroxyl groups show that La addition modifies them appreciably, decreasing the band strength and shifting slightly to lower frequency the most intense one. Furthermore, no relevant modification is found after Ni addition.

3.1.5. XPS analysis

In Fig. 5 the XP spectra are reported in the Al(2p) and Ni(3p) region. The Al(2p) spectrum of the LA is similar to that reported for γ-Al_2O_3 [30,31], showing a single peak at ca 74.2 eV. The Al(2p) spectra of both NiA and NiLA show a significant shift of the main peak down to 73.9 eV while an additional component is evident at 68,9 eV in the NiA sample, shifting to 68.0 eV in the NiLA sample, which is due to Ni(3p) transition of oxidized Ni [32].

The XP spectrum of the LA and NiLA samples in the 830–845 eV region (Fig. 6) is due to lanthanum 3d5/2 transition. The peak positions we found in the case of LA sample at 836.0 eV and 839.5 eV are at slightly higher energies than those reported for bulk $La(OH)_3$ [33] and, even more, than those reported for La_2O_3 [33–35], $LaAlO_3$ [33,35]. and a number of La hexaaluminates [36–38]. This splitting is a consequence of two different final states in the photon emission, and as result of hybridization of 4f orbitals of La atoms with surrounding atoms ($3d^94f^1$ and $3d^94f^0$ final states, for higher and lower binding energy peaks, respectively). The peak position in our spectrum is even more shifted to higher energies than those reported for other La/Al_2O_3 samples [35]. As reported by Ferrandon and Björnbom [33] the La 3d5/2 signal is found at slightly higher energy for dispersed La^{3+} than for stoichiometric compounds. Thus this finding supports the idea that La disperses on the surface of alumina on our LA sample without forming compound structures.

The addition of Ni results in a shift to lower energies of both peaks due to the lanthanum 3d5/2 transition, now observed at 835.0 and 838.5 eV, in agreement with previous results [15]. This shift should be considered as evidence of some Ni–La interaction.

The XP spectrum of the NiA sample in the Ni 2p3/2 (830–865 eV) (Fig. 7, up) shows two main peaks at 856.1 and 862.3 eV which compare quite well with the spectra reported of $NiAl_2O_4$, and Ni/Al_2O_3 samples [39] and $LaNiAl_{11}O_{19}$ [37,38] and are assigned to a nickel (2+) component and its satellite line (ca 862 eV).

The XP spectra in the La 3d3/2 and Ni 2p3/2 (830–860 eV) partially overlap (Fig. 7, down) and must be discussed together for the sample NiLA. The Ni 2p3/2 components are observed at 855.6 and 861.8 eV both slightly shifted with respect to the positions observed for NiA while the components at 851.7 and 865.1 eV are assigned to La 3d3/2 plasmon component.

The overall XPS features suggest that La disperses in a quite disordered way on alumina in LA and NiLA samples, and that a substantial Ni–La interaction occurs in the case of NiLA sample.

3.1.6. Temperature programmed reduction (TPR) of Ni-containing catalysts

H_2-TPR data of nickel containing samples are reported in Fig. 8 and Table 1. In both cases the largely predominant peak is centered at 1073 K corresponding to a complete reduction of Ni oxidized species to the metallic state. The slight apparent excess of hydrogen consumption with respect to the expected 1:1 stoichiometry (assuming Ni as Ni^{2+}), observed in both cases, might be due to possible adsorbed or spilled over hydrogen [40]. The onset of reduction is observed near 740 K for both catalysts, but lanthanum-free sample shows a weak consumption peak centered near 830 K less or

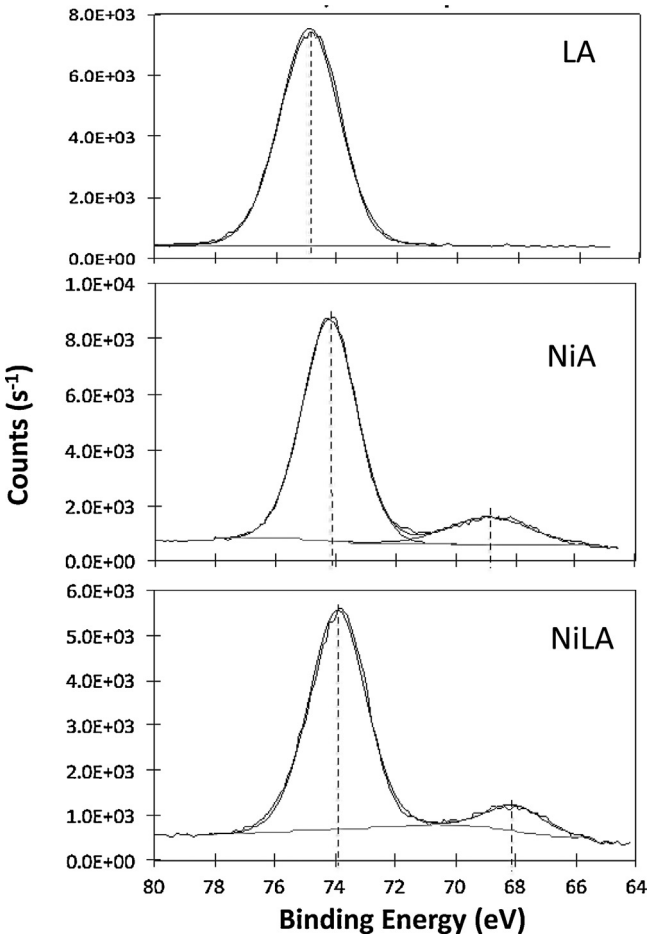

Fig. 5. XP spectra of LA, NiA and NiLA in the Al(2p) and Ni(3p) binding energy region 80–64 eV.

not evident for NiLA. This suggests that a small population of more easily reducible Ni species is present on NiA, maybe small NiOx clusters. In any case, neither TPR curve shows the peak associated with free NiO, typically centered at 500–800 K. The shift to higher reduction temperature values than for other Ni samples prepared

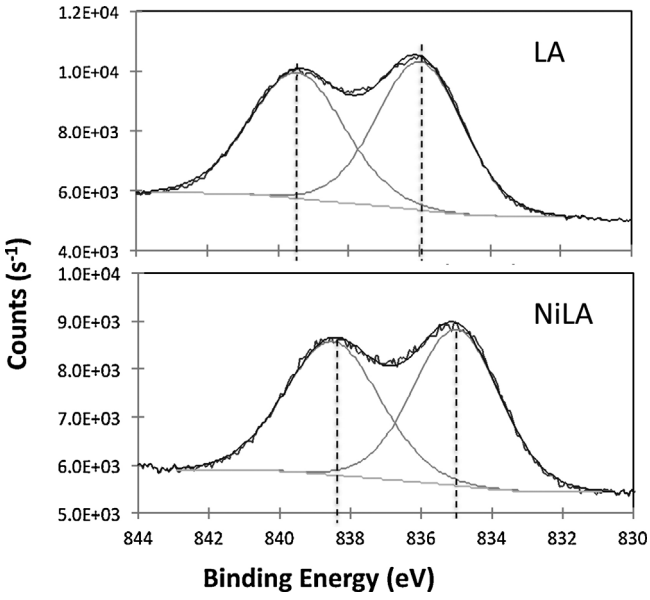

Fig. 6. XP spectra of LA and NiLA in the La(3d5/2) binding energy range 844–830 eV.

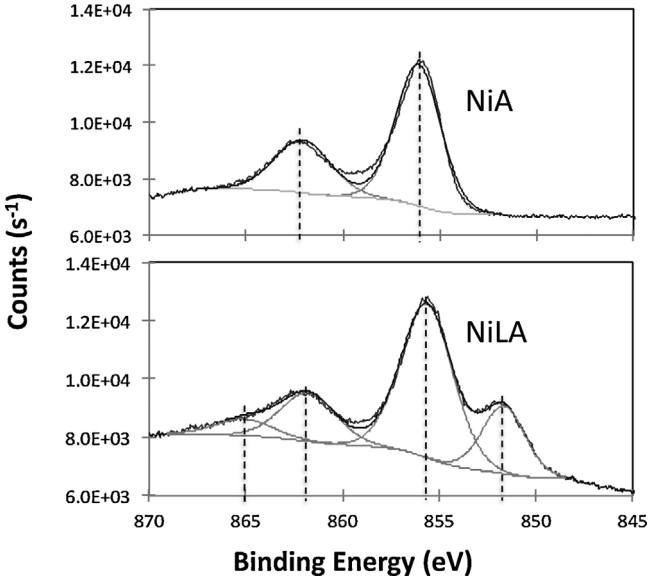

Fig. 7. XPS spectra of NiA and NiLA in the Ni(2p3/2) binding energy region 870–845 eV.

with an alumina support containing some silica [13] indicates a less reducible nickel species (nickel aluminate and/or lanthanate). This is in accordance with UV–vis and XRD analysis discussed above.

3.2. Catalytic activity studies

3.2.1. Ethanol temperature programmed surface reaction (TPSR)

Ethanol TPSR curves on the LA catalyst are reported in Fig. 9. The data show that conversion of ethanol starts just above 630 K producing mostly ethylene, with small amounts of diethylether (peak at 753 K), acetaldehyde (peak at 810 K) and CH_4, CO and CO_2 in increasing amounts above 830 K. Thus, dehydrating activity is largely predominant as found also on pure alumina with high selectivity but at lower temperature [41] as well as on pure lanthana, where lower amounts of acetaldehyde are formed and reaction occurs at slightly higher temperature [42].

Ethanol TPSR on unreduced NiA (Fig. 10, left) shows a similar conversion curve shifted to lower temperatures, with ethylene as the main product at high temperature and diethylether production limited to the 550–770 K range. A small peak with pro-

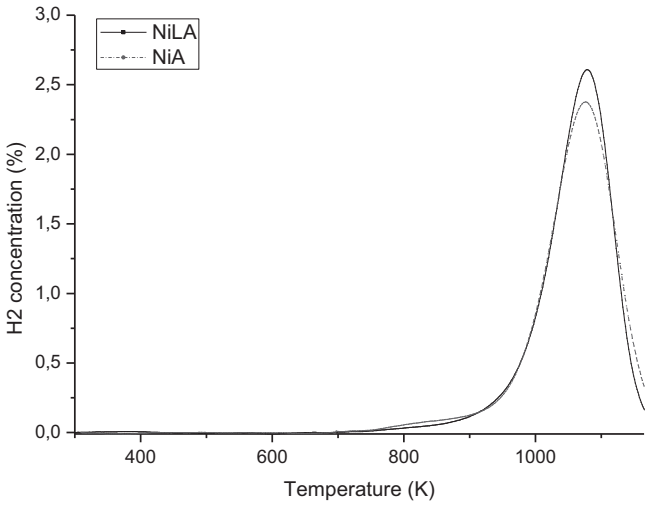

Fig. 8. H_2-TPR of NiA and NiLA samples.

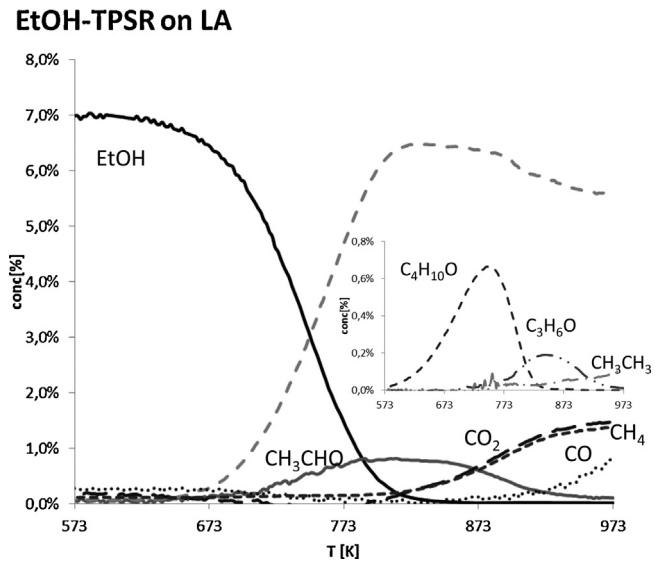

Fig. 9. Ethanol TPSR on LA sample: composition profile for each product detected.

duction of acetaldehyde is centered 790 K. Pre-reduction of NiA (Fig. 10, right) results in important changes. In particular, at 690 K sharp peaks are observed due to CH_4 and CO, associated to the ethanol decomposition reaction typically observed on Ni metal particles at moderate temperatures [43]. Additionally, at high temperature ethylene selectivity drops in favor of CO and CO_2. It should be noted that in this case an increase of the pressure was recorded, up to 4 psi at the maximum temperature thus suggesting that some coke deposition occurs due to ethylene polymerization.

Ethanol TPSR on unreduced NiLA (Fig. 11, left) shows also a similar conversion curve but much higher selectivity to acetaldehyde with a maximum near 780 K, and the production of acetone too (peak at 830 K), reducing drastically the production of diethylether, whose maximum is now at 673 K. Also after pre-reduction (Fig. 11, right) sharp peaks are observed due to CH_4 and CO, this time at a slightly higher temperature (720 K) associated with the ethanol decomposition. At higher temperatures ethylene, acetaldehyde, CO and CO_2 are the main products.

These data show that the presence of lanthanum significantly modifies the state of both unreduced and reduced catalysts, reducing dehydration activity to ethylene. The effect of La addition to catalyst formulation is also underlined by the fact that no pressure drop was observed in this case such suggesting limited coking during the TPSR of ethanol. This is possibly due to the reduced acidity (or enhanced basicity) of the support due to lanthanum addition, as shown above by the IR study of CO_2 adsorption. The presence of lanthanum also increases the dehydrogenation to acetaldehyde, which is a typical reaction occurring both on basic catalysts (La oxide component) and on reducible catalysts (Ni^{2+} component) [44].

3.2.2. Ethanol steam reforming (ESR)

In Table 2 the catalytic activity of NiA in the conversion of ethanol in the presence of steam is reported. In steady-state experiments conducted in the ascending temperature mode, the ethanol conversion is very low with diethylether as the main product at both 523 and 573 K. In the temperature range 673–973 K conversion comes to completion, with dehydration of ethanol to ethylene being largely the major reaction, together with some dehydrogenation to acetaldehyde, decomposition and steam reforming. This catalyst appears to be, in the ascending temperature experiment, definitely less active than a similar sample prepared with an alumina support containing a small silica amount [12,13]. However, after leaving the sample for 4 h at 1023 K, in the descending temperature mode, ESR occurs with total selectivity to CO_x and very high hydrogen yield (87%). This suggests that reduction/conditioning of the catalyst is much slower for this catalyst with respect to the silica-containing one, studied previously, in agreement with the different TPR curves [13]. Very high ESR activity is retained until 873 K where some methane starts to form, thus lowering the hydrogen yield to 0.80. At 773 K ESR activity decreases to almost nil and dehydration to ethylene is the main reaction, while at lower temperature (573–523 K) dehydration to diethylether and dehydrogenation to acetaldehyde dominate.

This behavior can be understood based on the TPR experiment that shows how hard it is to reduce the catalyst. Only after some time on stream at 1023 K is the catalyst reduced, thus generating active Ni metal centers. By decreasing the temperature, the kinetics of ESR slows down faster than the rate of dehydration and dehydrogenation, which become predominant.

As reported in Table 3 in the case of NiLA catalyst complete and very selective ESR activity is obtained already at 973 K in the

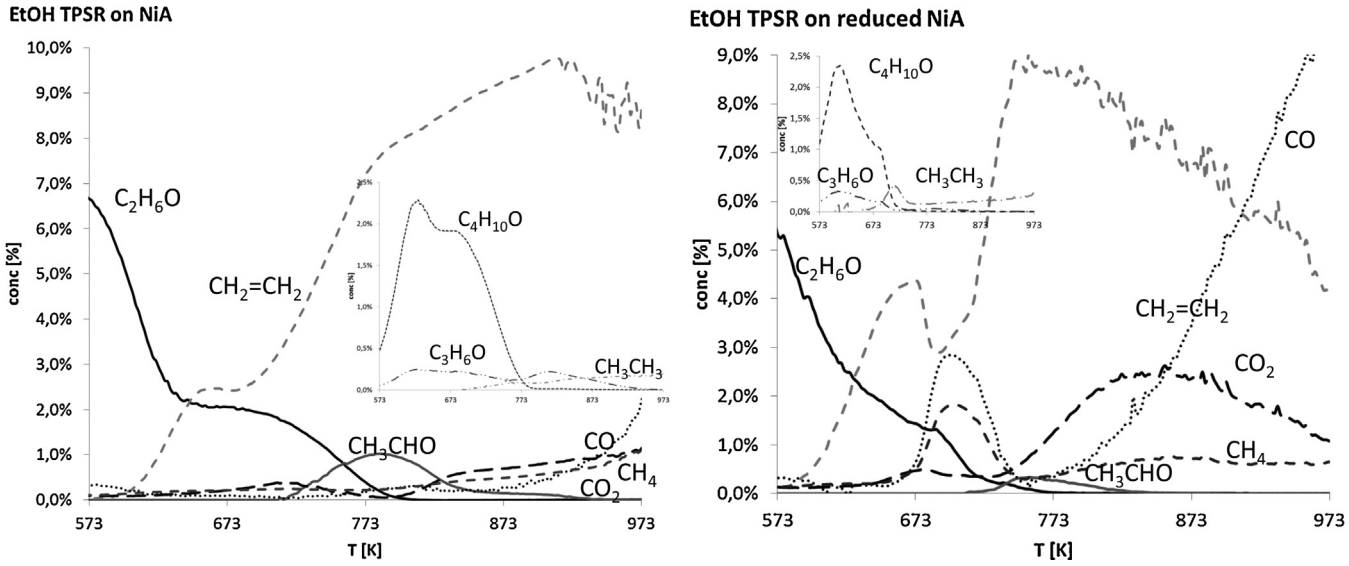

Fig. 10. Ethanol TPSR on NiA sample: composition profile for each product detected on the unreduced catalysts (left) and pre-reduced one (right).

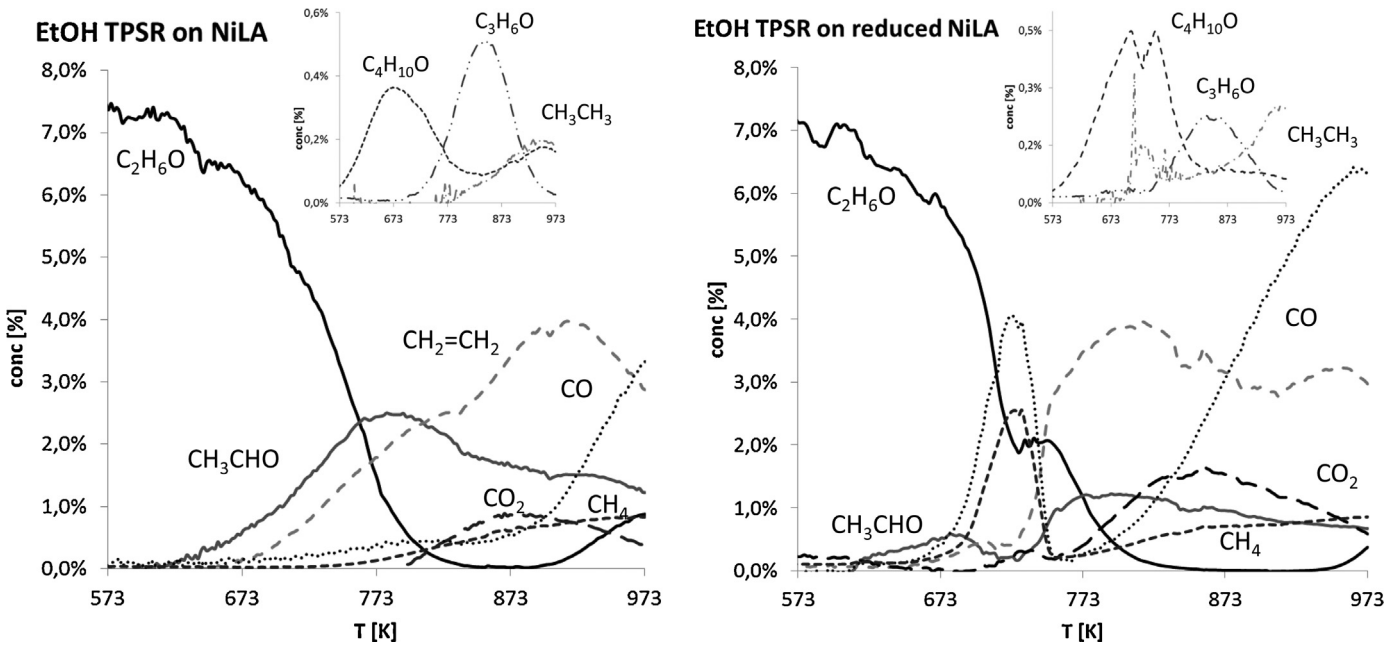

Fig. 11. Ethanol TPSR on NiLA sample: composition profile for each product detected on the unreduced catalysts (left) and the prereduced one (right).

ascending temperature mode, with 90% hydrogen yield. This catalytic activity for ESR is essentially retained down to 873 K in the descending temperature experiment. We have to mention that the surface area of NiLA is lower than that of NiA while the Ni content is the same. Thus, Ni agglomeration can be higher on NiLA than on NiA and this can also affect favorably the reducibility and catalytic activity.

At lower temperatures, however, the NiLA catalyst is more active in the dehydrogenation of ethanol to acetaldehyde than in the dehydration reactions to ethylene and diethylether, unlike the NiA catalyst. This dehydrogenation activity is also certainly associated with Ni species, thus suggesting that La addition modifies the activity of part of the Ni centers, possibly highly dispersed Ni^{2+} ions. On the other hand, in the ascending temperature experiment, acetone is also observed in significant yields (0.25 at 873 K) when steam reforming had not yet occurred. This activity almost disappeared in the descending temperature experiments. In fact, much less acetone is formed on reduced NiLA upon ethanol TPSR that on fresh NiLA. Thus, this activity can be mainly attributed to unreduced catalyst, still not "conditioned" for steam reforming.

3.2.3. Conversion of ethanol/phenol/water mixture

When ethanol, phenol and water are fed together on the fresh NiA catalyst (Table 4), the main reactions at low temperature are ethanol dehydration to ethylene, ethanol dehydrogenation to acetaldehyde and phenol alkylation by ethanol to ethylphenols (eight carbon compounds, C8). At 973 K some ethanol steam reforming occurs but phenol conversion is very low. The situation changes at 1023 K where both organic reactants are fully converted to CO_2, CO and hydrogen, with a hydrogen yield of 0.82. By decreasing the temperature the catalyst remains conditioned, thus retaining high steam reforming activity also at 973 K (H_2 yield 0.84). At 873 K conversion of phenol is decreased but still steam reforming largely predominates, while at 773 K steam reforming activity decreases very much, ethylene and alkylates are formed in significant amounts.

Table 2
Ethanol steam reforming dynamic data on NiA in terms of conversion (X_i), hydrogen yield (Y_{H2}) and selectivities (S_i) to carbon products in the ascending and descending temperature mode.

	ESR increasing temperature experiment on NiA											
T Furnace (K)	X C_2H_5OH	X H_2O	Y H_2	S CH_4	S CO	S CO_2	S C_2H_4	S C_2H_6	S C_3H_6	S C_2H_4O	S $C_4H_{10}O$	S $C_4H_8O_2$
523	0,02	0,00	0,00	0,00	0,00	0,00	0,00	0,00	0,00	0,10	0,90	0,00
573	0,04	0,00	0,00	0,00	0,00	0,00	0,10	0,00	0,01	0,03	0,86	0,01
673	0,59	−0,06	0,03	0,00	0,06	0,00	0,55	0,02	0,00	0,04	0,31	0,01
773	1,00	−0,15	0,02	0,00	0,00	0,01	0,93	0,00	0,01	0,03	0,02	0,00
873	1,00	−0,14	0,03	0,01	0,01	0,03	0,83	0,06	0,02	0,01	0,04	0,00
973	1,00	−0,10	0,08	0,05	0,07	0,04	0,65	0,06	0,01	0,13	0,00	0,00
1023	0,95	0,09	0,38	0,15	0,40	0,19	0,18	0,04	0,00	0,04	0,00	0,00
	ESR decreasing temperature experiment on NiA											
T Furnace [K]	X C_2H_5OH	X H_2O	Y H_2	S CH_4	S CO	S CO_2	S C_2H_4	S C_2H_6	S C_3H_6	S C_2H_4O	S $C_4H_{10}O$	S $C_4H_8O_2$
1023	1,00	0,37	0,87	0,00	0,39	0,60	0,00	0,00	0,00	0,00	0,00	0,00
973	1,00	0,38	0,87	0,00	0,36	0,64	0,00	0,00	0,00	0,00	0,00	0,00
873	1,00	0,36	0,80	0,08	0,25	0,66	0,00	0,00	0,00	0,00	0,00	0,00
773	1,00	0,02	0,27	0,01	0,03	0,26	0,63	0,05	0,00	0,01	0,00	0,00
673	0,79	−0,10	0,03	0,00	0,01	0,04	0,79	0,05	0,00	0,05	0,06	0,00
573	0,17	−0,01	0,01	0,00	0,01	0,01	0,15	0,00	0,00	0,13	0,69	0,00
523	0,04	0,00	0,00	0,01	0,01	0,02	0,01	0,02	0,02	0,49	0,45	0,00

Table 3
Ethanol Steam reforming steady-state data on NiLA in terms of conversion (X_i), hydrogen yield (Y_{H2}) and selectivities (S_i) to carbon products in the ascending and descending temperature mode.

	ESR increasing temeperature experiment in NiLA													
T (K)	X C_2H_5OH	X H_2O	Y H_2	S CH_4	S CO	S CO_2	S C_2H_4	S C_2H_6	S C_3H_6	S C_2H_4O	S $C_4H_{10}O$	S $C_4H_8O_2$	S C_3H_6O	S $C_5H_{10}O$
523	0,01	0,00	0,00	0,00	0,00	0,00	0,00	0,00	0,00	0,07	0,93	0,00	0,00	0,00
573	0,02	0,00	0,00	0,00	0,00	0,00	0,01	0,00	0,05	0,10	0,84	0,01	0,00	0,00
673	0,22	0,00	0,04	0,00	0,00	0,10	0,28	0,00	0,01	0,29	0,16	0,09	0,08	0,00
773	0,90	0,01	0,20	0,00	0,00	0,17	0,36	0,00	0,05	0,14	0,04	0,01	0,20	0,05
873	0,98	0,00	0,22	0,01	0,04	0,14	0,36	0,03	0,03	0,10	0,01	0,00	0,26	0,01
973	1,00	0,40	0,90	0,00	0,29	0,71	0,00	0,00	0,00	0,00	0,00	0,00	0,00	0,00
1023	1,00	0,32	0,78	0,05	0,39	0,54	0,00	0,00	0,00	0,00	0,00	0,00	0,00	0,00
	ESR decreasing temperature experiment on NiLA													
T(K)	X C_2H_5OH	X H_2O	Y H_2	S CH_4	S CO	S CO_2	S C_2H_4	S C_2H_6	S C_3H_6	S C_2H_4O	S C_3H_6O	S $C_4H_{10}O$	S $C_4H_8O_2$	
1023	1,00	0,34	0,83	0,01	0,45	0,53	0,00	0,00	0,00	0,00	0,00	0,00	0,00	
973	1,00	0,37	0,85	0,02	0,37	0,62	0,00	0,00	0,00	0,00	0,00	0,00	0,00	
873	1,00	0,37	0,82	0,08	0,24	0,69	0,00	0,00	0,00	0,00	0,00	0,00	0,00	
773	0,84	0,22	0,52	0,16	0,21	0,52	0,03	0,03	0,00	0,04	0,00	0,02	0,00	
673	0,29	0,04	0,12	0,13	0,17	0,29	0,03	0,01	0,00	0,32	0,01	0,03	0,00	
573	0,03	0,00	0,01	0,04	0,05	0,12	0,01	0,00	0,00	0,72	0,00	0,04	0,02	
523	0,01	0,00	0,00	0,02	0,02	0,06	0,00	0,00	0,00	0,90	0,00	0,00	0,00	

In the case of the NiLA catalyst (Table 5), steam reforming of both ethanol and phenol (EPSR) is already occurring in the ascending temperature experiment at 973 K, although phenol conversion is still not complete. In the descending temperature experiment, almost full conversion of both reactants is still observed at 873 K. The hydrogen yields obtained are even higher than those obtained on NiA mainly due to a higher CO_2 to CO ratio. CO and CO_2 production can be associated to the establishing of the water gas shift/reverse water gas shift equilibrium, or can be due to parallel paths. Taking into account that we produce more CO_2 and less CO than that calculated from thermodynamics, we can conclude that the NiLA catalyst is either less active in catalyzing the reverse water gas shift reaction, or more active in a direct way to CO_2 not involving CO as an intermediate.

3.2.4. Conversion of ethanol/phenol/water mixture in the presence of sulfur

For this experiment the best catalysts at 973 K in the ascending temperature experiment was chosen, NiLA, also to look at the effect of lanthanum in the presence of sulfur. As previously done, we used a non-toxic molecule tetrahydrothiophene (THT) as a sulfur-containing agent. We previously showed that THT indeed gives rise to H_2S in reaction conditions [21]. In Fig. 12 the results concerning the effect of sulphur in the conversion of ethanol and phenol in the presence of water on the NiLA catalyst are reported. In this case the catalyst was previously tested at 1023 K for 30 min in the reactant mixture and then taken to the lower operation temperature (973 K), until steady state was reached. The pulse of 0.011 mol_S/mol_{Ni} already produces a partial poisoning of the catalyst that became very pronounced by further introduction of 0.033 mol_S/mol_{Ni}.

The first pulse results in a decrease of conversion of both reactants (but definitely more important for phenol than for ethanol) and a definite slowdown of steam reforming activity together with a reappearance of ethanol dehydration activity to ethylene and also some dehydrogenation to acetaldehyde. Further introduction of THT strongly increases all these effects, while time on stream with sulfur-free feed allows a progressive partial recovery of the previous activity. Additionally an inversion of selectivity between CO and CO_2 is also observed.

The comparison with the results of similar experiments performed on Ni16 and NiMg catalysts shows that this catalyst is even more sensitive to sulfur than the others.

3.3. Characterization of the spent catalysts

3.3.1. XRD

Fig. 13 shows the XRD patterns of used NiA and NiLA coming from ethanol steam reforming reaction. The broad feature around $2\theta = 25^\circ$ in both samples is due to the presence of silica glass, used

Table 4
Ethanol phenol steam reforming steady-state data on NiA in terms of conversion (X_i), hydrogen yield (Y_{H2}) and carbon selectivities (S_i) to carbon products in the ascending and descending temperature mode.

	Increasing temperature experiment NiA														
T (K)	C Conversion	X C_2H_5OH	X C_6H_6O	X H_2O	Y H_2	S CH_4	S CO	S CO_2	S C_2H_4	S C_2H_6	S C_3H_6	S C_2H_4O	S $C_4H_{10}O$	S C_6H_6	S C_8
773	0,47	0,94	0,14	−0,05	0,01	0,00	0,00	0,00	0,62	0,01	0,01	0,14	0,01	0,00	0,22
873	0,15	0,42	0,02	−0,02	0,01	0,00	0,00	0,00	0,55	0,02	0,04	0,30	0,00	0,00	0,11
973	0,19	0,40	0,05	0,01	0,05	0,05	0,11	0,14	0,29	0,00	0,03	0,31	0,00	0,06	0,00
1023	1,00	1,00	1,00	0,46	0,82	0,00	0,46	0,54	0,00	0,00	0,00	0,00	0,00	0,00	0,00
	Decreasing temperature experiment NiA														
T(K)	C Conversion	X C_2H_5OH	X C_6H_6O	X H_2O	Y H_2	S CH_4	S CO	S CO_2	S C_2H_4	S C_2H_6	S C_3H_6	S C_2H_4O	S $C_4H_{10}O$	S C_6H_6	S C_8
1023	1,00	1,00	1,00	0,47	0,83	0,00	0,44	0,56	0,00	0,00	0,00	0,00	0,00	0,00	0,00
973	1,00	1,00	1,00	0,48	0,84	0,00	0,40	0,60	0,00	0,00	0,00	0,00	0,00	0,00	0,00
873	0,88	1,00	0,81	0,38	0,66	0,07	0,27	0,61	0,05	0,00	0,00	0,00	0,00	0,00	0,00
773	0,44	0,66	0,30	0,11	0,22	0,03	0,05	0,45	0,18	0,01	0,03	0,02	0,01	0,00	0,23

Table 5
Ethanol phenol steam reforming steady-state data on NiLA in terms of conversion (X_i), hydrogen yield (Y_{H2}) and carbon selectivities (S_i) to carbon products in the ascending and descending temperature mode.

	EPSR increasing temperature experiment NiLA																	
T (K)	C Conversion	X C_2H_6O	X C_6H_6O	X H_2O	Y H_2	S CH_4	S CO	S CO_2	S C_2H_4	S C_2H_6	S HCHO	S C_3H_6	S CH_3COH	S C_3H_6O	S $C4H_{10}O$	S C_6H_6	S C_7	S C_8
773	0,49	0,91	0,24	0,00	0,07	0,00	0,00	0,08	0,14	0,01	0,02	0,03	0,11	0,19	0,02	0,01	0,02	0,38
873	0,34	0,70	0,08	−0,02	0,04	0,01	0,02	0,06	0,44	0,00	0,02	0,01	0,26	0,01	0,00	0,00	0,00	0,17
973	0,90	1,00	0,84	0,42	0,76	0,01	0,36	0,61	0,00	0,00	0,00	0,00	0,00	0,00	0,00	0,00	0,00	0,02
1023	0,93	1,00	0,88	0,47	0,82	0,00	0,31	0,69	0,00	0,00	0,00	0,00	0,00	0,00	0,00	0,00	0,00	0,00

	EPSR decreasing temperature experiment NiLA												
T (K)	C Conversion	X C_2H_6O	X C_6H_6O	X H_2O	Y H_2	S CH_4	S CO	S CO_2	S C_2H_4	S C_2H_6	SHCHO	S C_3H_6O	S C_8
1023	1,00	1,00	1,00	0,51	0,88	0,00	0,31	0,69	0,00	0,00	0,00	0,00	0,00
973	1,00	1,00	1,00	0,47	0,84	0,01	0,42	0,57	0,00	0,00	0,00	0,00	0,00
873	0,98	0,99	0,98	0,46	0,75	0,07	0,22	0,67	0,01	0,03	0,00	0,00	0,00
773	0,33	0,51	0,21	0,09	0,19	0,02	0,08	0,51	0,09	0,01	0,02	0,01	0,25

as diluent in the experiments. The peak around 26–27° is related to the formation of graphitic carbon [45]. In both samples the presence of alumina and of cubic nickel (JCPDS Table 04-0850) is observed. Similar results are obtained for samples used in the EPSR experiments. We note that in a previous study [25] the metastable hexagonal polymorph of Ni was found in the used Ni/Al_2O_3 catalyst after an ESR experiment. However in that case the maximum temperature used for reaction was 773 K, while in this case the catalyst had been tested up to 1023 K. It is likely that hexagonal Ni may transform into the thermodynamically stable cubic form at higher temperatures. An evaluation of the amount of graphitic carbon deposited on the two catalysts was made by comparing the intensity of the peaks at $2\theta = 26.1°$ with the peak of Ni ($2\theta = 52.1°$) and that at $2\theta = 63.8°$ due to alumina or to aluminate, which have similar intensities. These ratios are higher for NiA than for NiLA by a factor 1.5–2, suggesting that the presence of lanthanum decreases the amount of graphitic carbon formed. This finding compares well with the weight increase measured for the catalytic beds, upon ESR reaction: $\Delta w_{NiA} \sim 2\ \Delta w_{NiLA}$. It is supposed that graphitic carbon is mainly formed on the support by polymerization/carbonization of ethylene.

3.3.2. FE-SEM

In Figs. 14 and 15, FE-SEM images of the NiLA catalyst after ESR and EPSR experiments, respectively, are shown. The images on the left side were recorded using the back-scattered electrons in order to take advantage of the compositional contrast; images of the morphologies of the same samples (Fig. 13 right) were recorded using an InLens detector. In both cases particle aggregates where Ni and La appear to be dispersed (continuous brilliant regions) are seen, free of apparent carbon materials, while in other regions carbon nanotubes containing Ni particles are easily detectable. This agrees with the well- known ability of Ni particles to cause the growth of carbon nanotubes during steam reforming reactions [46]. A rough inspection of the figures suggests that the amount of carbon nanotubes formed on NiA and NiLA is similar. In both cases it seems that only the fraction of nickel which forms “free” Ni particles participate to the formation of carbon nanotubes.

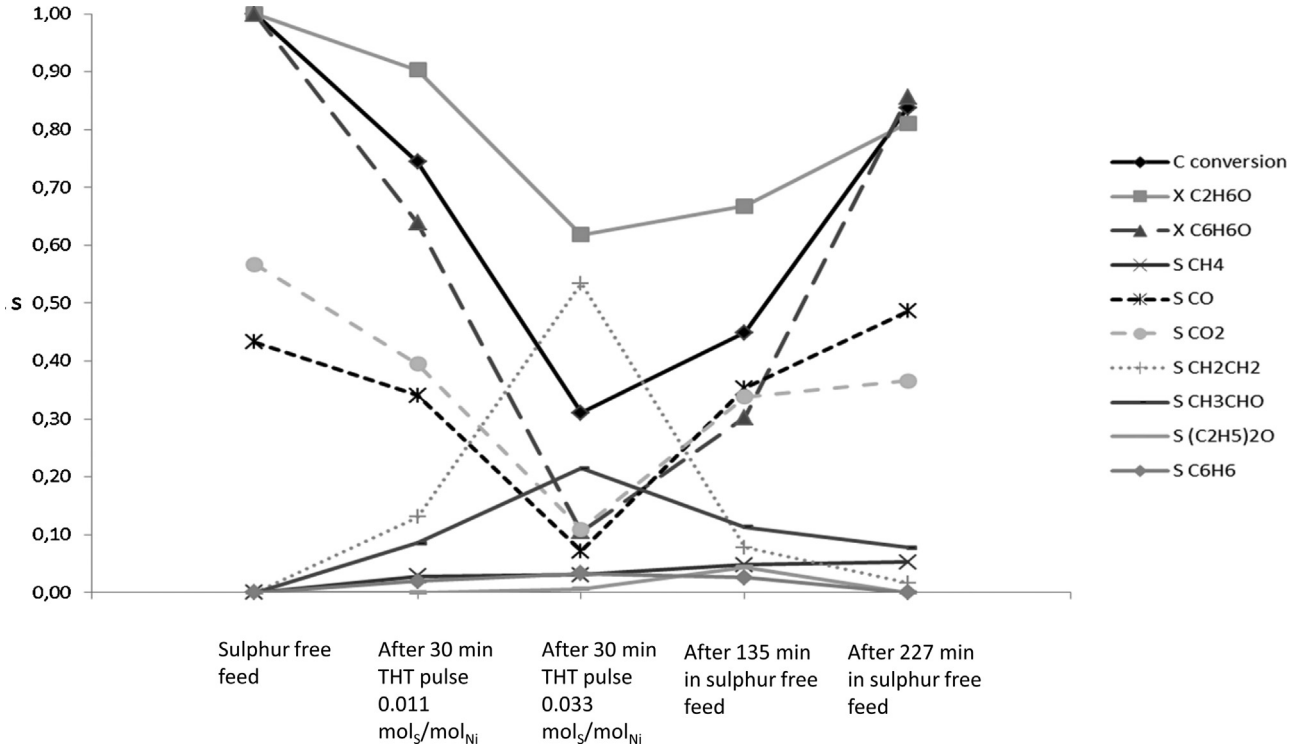

Fig. 12. Sulfur poisoning experiment with THT pulses: conversion (Xi) and carbon based selectivity (Si) at 973 K.

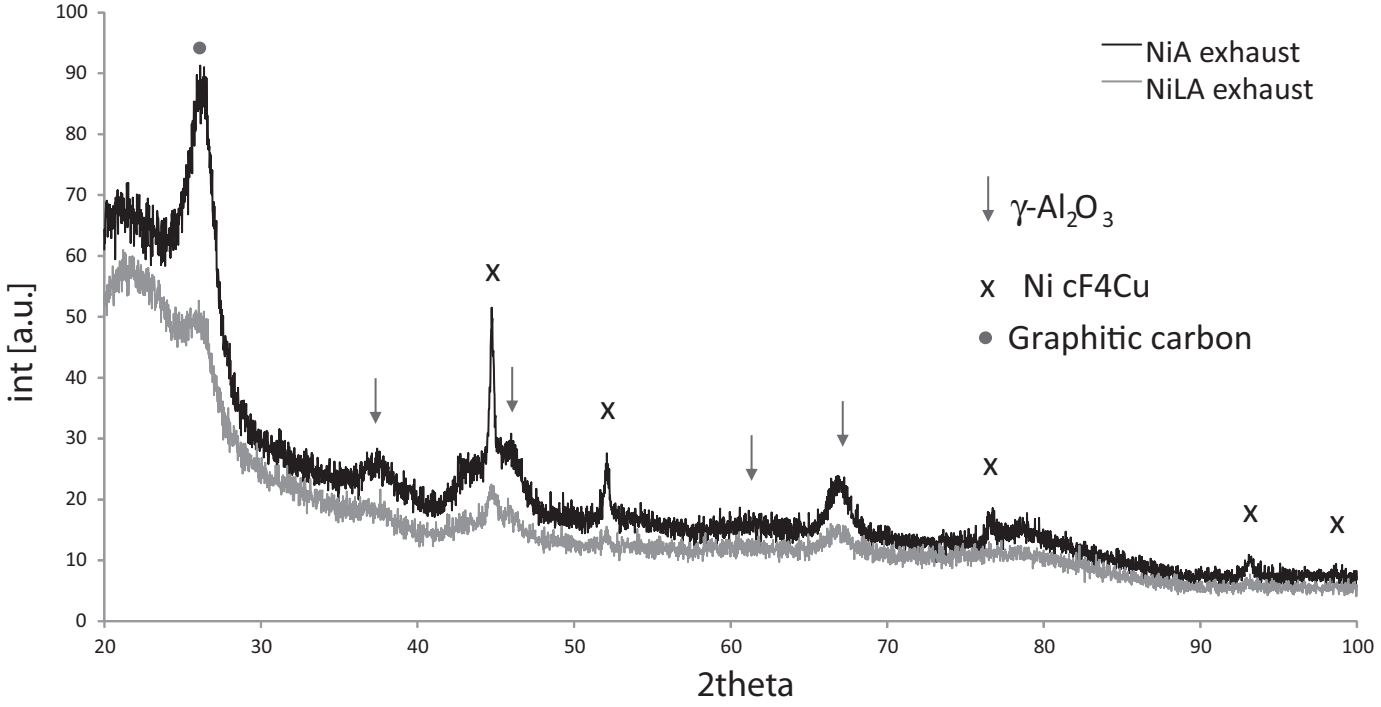

Fig. 13. XRD diffraction pattern of spent material after Ethanol Steam Reforming experiment.

4. Discussion

The data reported here show that both NiA and NiLA catalysts are active for the ESR and EPSR reactions. The data reported here for ESR reaction are reasonably consistent with those reported previously on similar catalysts [16,47,48], where the subject of catalyst conditioning and sulfur deactivation were not taken into account. Our results allow some further discussion on the reaction path. In all cases "conditioned catalysts", i.e., catalysts exposed to the feed up to 1023 K, retain almost full SR activity for both reactions down to 873 K producing only carbon oxides and hydrogen. Hydrogen yields ≥ 0.8 are obtained upon ESR at 873 K with such "conditioned" catalysts, while the hydrogen yield is lower upon EPSR (0.66–0.75) due to the formation of methane, ethylene and ethane. We note that the water-to-carbon ratio used in the feed is only slightly lower in the EPSR (2.73) than in the ESR experiments (3.0), and is, in both cases, in large stoichiometric excess. Previous studies performed using both flow reactor steady-state experiments and IR spectroscopy [49] allowed us to conclude that, while ethylene and methane and, to a lesser extent, ethane, are frequently produced upon ESR, the SR of phenol does not produce any detectable organic species except small amounts of benzene [12,49]. Another effect of the presence of phenol is to reduce the conversion of ethanol at $T < 873$ K over both catalysts, even if this effect is reduced on NiLA. This effect can be due to competition of ethanol and phenol for the same adsorption sites; the data indicate that ethanol steam reforming is faster than phenol steam reforming in the range 773–873 K, the former starting at lower temperatures than the latter. The possible conclusion is that phenol either shifts ethanol over less selective sites for ESR, or limits the adsorption of water. In fact, water, ethanol and phenol have a similar functionality (the hydroxyl- group) which is involved in the first adsorption step. However, while ethanol and water have similar volatilities and acido-basicity, phenol is far less volatile and is more acidic.

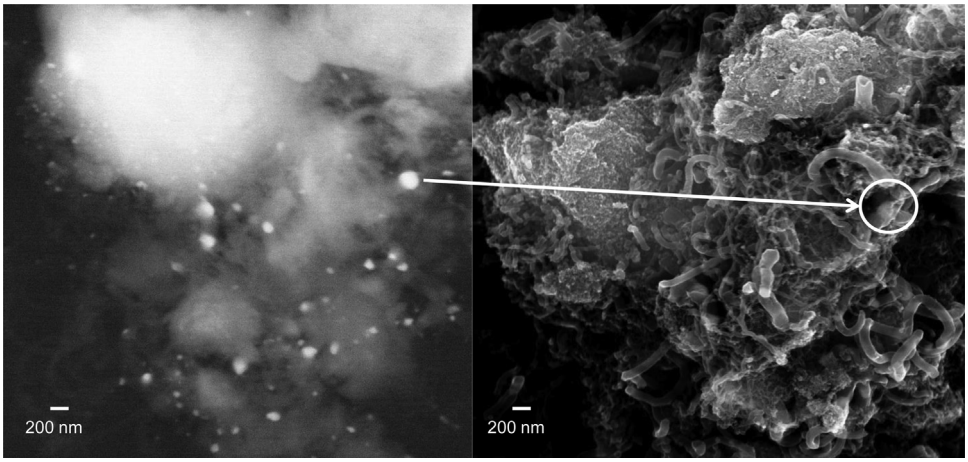

Fig. 14. FE-SEM micrographs of NiLA sample after ethanol steam reforming experiment, recorded with backscattered electrons detector (left) and with InLense detector (right).

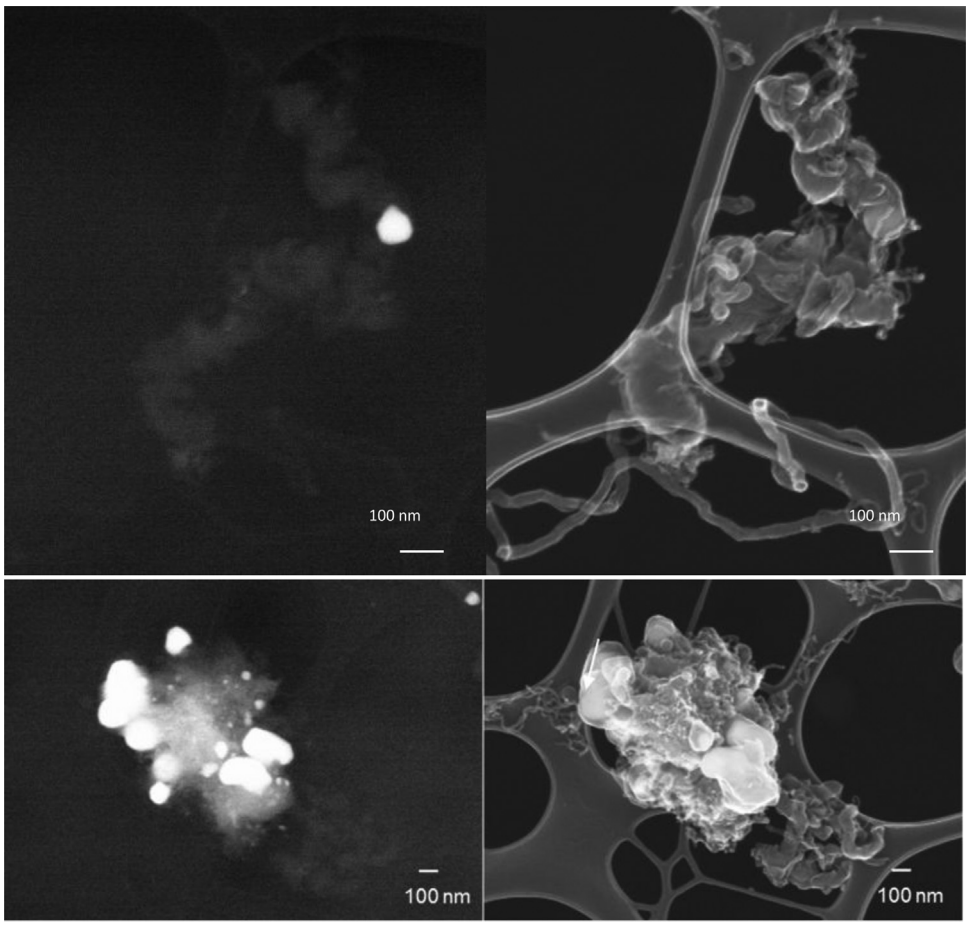

Fig. 15. FE-SEM micrographs of NiLA sample after ethanol/phenol steam reforming experiment, recorded with backscattered electrons detector (left) and with InLense detector (right).

Thus, phenol adsorption can be stronger, limiting the availability of adsorbed and "activated" water for SR.

When comparing NiA and NiLA catalysts in ESR, it becomes evident that a different yield of byproducts is obtained in conditions where ESR still does not occur or is not complete. Over the conditioned NiA catalyst, ethylene is largely the main byproduct at 673–873 K while diethylether is the main byproduct at 523–573 K. This is the typical reactivity of alumina, producing with high selectivity diethylether at lower temperatures and ethylene at higher temperatures from ethanol [50]. Instead, over the conditioned NiLA, acetaldehyde is the predominant byproduct, indicative of the dehydrogenation reaction pathway. Finally, when ESR is running but is slow (i.e., at 673 and 773 K), the conversion of ethanol is higher on NiA than on NiLA.

The low-temperature catalyst behavior, when SR still does not occur,is confirmed by the ethanol TPSR experiments that clearly show that ethanol conversion is much slower on the reduced NiLA than on reduced NiA in the temperature range 573–673 K (Fig. 11 right). The addition of lanthanum also reduces strongly the yield to ethylene. The profiles in this temperature range are very similar for unreduced and reduced catalysts. On the other hand, only ethanol dehydration reactions take place on alumina, being associated to their Lewis acidic behavior [50]. In contrast, acetaldehyde formation from ethanol dehydrogenation is usually found on basic catalysts (such as lanthanum containing oxides) as well as on catalysts having redox activity (such as Ni^{2+}/Al_2O_3).

Thus, parallel reactions should run at 673–773 K, located in different sites:

1. ESR, catalyzed by reduced Ni species, mostly producing CO_2 and hydrogen

$$CH_3CH_2OH + 3H_2O \rightarrow 2CO_2 + 6H_2 \quad (1)$$

As discussed elsewhere [12], the amount of CO_2 obtained with Ni catalysts is higher than that calculated by thermodynamics for the water gas shift equilibrium. Thus, CO_2 is necessarily the primary product of the steam reforming reaction, whose stoichiometry is, consequently, that indicated in (1).

2. Ethanol dehydration reactions catalyzed by alumina:

$$2CH_3CH_2OH \rightarrow (CH_3CH_2)_2O + H_2O \quad (2)$$

$$CH_3CH_2OH \rightarrow CH_2 = CH_2 + H_2O \quad (3)$$

3. Ethanol dehydrogenation catalyzed by both $La–Al_2O_3$ and Ni^{2+}/Al_2O_3:

$$CH_3CH_2OH \rightarrow CH_3CHO + H_2. \quad (4)$$

These data suggest that the presence of lanthanum has the main effect of lowering the rate of the dehydration reactions, especially the production of ethylene (3). This favors the products of the competitive reactions (in terms of selectivity, not of activity which is overall decreased at temperatures below 873 K), including ESR.

Interestingly, TPSR profiles on the reduced catalysts show that the dehydration of ethanol is followed, on reduced catalysts, by a sharp step producing CH_4 and CO, nearly in 1:1 molar ratio. This step, found near 700 K on the reduced NiA and at a slightly higher temperature on the reduced NiLA (723 K) is not observed on

Table 6
Comparison of Ni based materials tested for ethanol phenol steam reforming in terms of phenol conversion and hydrogen yield at 873 and 773 K in descending temperature mode.

	Refs.		X_{C6H6O} 873 K	Y_{H2} 873 K	X_{C6H6O} 773 K	Y_{H2} 773 K
"Empty"	[12]	Quartz	0.03	0.02	0.25 – 0	0.01
Ni0	[12]	5% SiO_2–Al_2O_3	0.17 – 0.01	0.04 – 0.11	0.17 – 0.01	0.06 – 0
Ni5	[12]	5% Ni (5% SiO_2/Al_2O_3)	0.47	0.40	0.34	0.13
Ni16	[12]	16% Ni (5% SiO_2/Al_2O_3)	0.90	0.66	0.20	0.37
Ni39	[12]	39% Ni (5% SiO_2/Al_2O_3)	1.00	0.81	0.41	0.29
NiMg	[13]	16% Ni (20% MgO/5% SiO_2/Al_2O_3)	1.00	0.84	0.44	0.23
NiB	[13]	16% Ni (1%H_3BO_3/5% SiO_2/Al_2O_3)	0.57	0.25	0.02	0.11
BNi	[13]	1%H_3BO_3/16% Ni (5% SiO_2/Al_2O_3)	0.93	0.51	0.48	0.18
NiA	This work	16% Ni (Al_2O_3)	0.81	0,66	0.30	0,22
NiLA	This work	16% Ni (20% La_2O_3/Al_2O_3)	0.98	0.75	0.21	0.19

unreduced catalysts, thus it almost certainly involves reduced Ni species. It has already been reported [43] that extended Ni particles catalyze the ethanol decomposition reaction at low temperatures (ca 673 K):

$$CH_3CH_2OH \rightarrow CH_4 + CO + H_2. \quad (5)$$

According to our previous data, concerning high-content Ni catalysts and pure Ni nanoparticles [43], this reaction is the main one responsible for the formation of methane at low temperatures, thus reducing the selectivity to hydrogen in low- temperature ESR over Ni catalysts. This reaction does not occur on some Co catalysts and this is the reason for the higher selectivities in low- temperature ESR obtained on some Co catalysts than on Ni catalysts [51]. We note that methane is indeed found with significant selectivity over conditioned NiLA that produces much more methane also in the TPSR experiments, while is much less on NiA. Also this effect can be associated to the decrease of the rate of the competitive reaction converting ethanol to ethylene. The sudden disappearance of Reaction (5) observed in the TPSR experiment, Fig. 11 right maybe explained by poisoning of the active site. It seems possible to associate this phenomenon to the onset of the production of carbonaceous material, either graphitic carbon detected by XRD or carbon whiskers evident in FE-SEM microscopy.

On the other hand, all catalysts produce carbon nanotubes, at least when the Ni amount is sufficiently high. It seems in fact that carbon nanotubes form mainly over small Ni particles which are "separable" from the support. It should be noted as well that during ESR on NiA in descending temperature experiments, dehydration of ethanol is again the main reaction thus suggesting that alumina acid sites that give rise to ethanol dehydration are still not significantly deactivated (Reaction (3)) by coke deposition.

Therefore, the findings of this work indicate that most of the reaction products found result from parallel reactions occurring on different sites. They are not necessarily involved in the main mechanism of ESR. In any case most of these reaction by-products do not involve water as a reactant. It seems likely that the temperature onset for ESR activity is actually associated to that of the activation of water. Thus the main factor determining high activity in steam reforming reactions should be associated to the reducibility of the oxide particles; may be the sizes of the resulting metal particles might determine the minimum temperature for the activation of water. In Table 6 the behavior of the "conditioned" catalysts at 873 K and 773 K is compared with those of other catalysts previously studied in the same conditions, and prepared with closely similar but not identical procedures. At 873 K the conversion of both C-containing reactants is very high in all cases and steam reforming is the predominant reaction. At 773 K, in all cases the phenol conversion is limited and several reactions run together with EPSR. The hydrogen yield is used to compare their activities. The data show that the Ni–Mg catalyst on a silica-containing alumina support is the best among the catalysts studied. The silica-free alumina support does not produce a better catalyst than the silica-containing support, while the addition of lantana promotes the catalyst activity, although not strongly.

The modifier used in our investigations (Mg [13], B [13] and SiO_2 [12], La) plays a main role in modifying the properties of the alumina support and consequently the parallel reactions occurring there but it may also have an important role in determining the structure and stability of the nickel oxide particles, and therefore, the activation of water for the key ESR reaction. It is possible that spillover effects, as suggested for other catalysts [52], can be a key feature in the steam reforming reaction over supported metal catalysts: activation of water could occur on the support [13] giving rise to active hydroxyl- or oxy-groups, whose activity can be crucial for determining the oxidation state of the metal particles and/or to provide the active sites for the SR reaction.

In regard to our findings with the addition of the THT sulfur species in the gas mixture; namely that all catalysts we studied here were deactivated by sulfur, we must invoke the poisoning of the metallic nickel ESR sites as the main reason. The activation of the parallel reactions producing by-products, i.e., mainly ethylene and acetaldehyde, but also methane and benzene, was not affected in the presence of sulfur. This selective site poisoning is another way to demonstrate the parallel reaction scheme on different (metallic/non metallic nickel) sites proposed above. The lack of nickel sites turns off the ESR reaction even on catalysts modified with basic elements such as Mg and La. We note here that the amount of La we used in the formulation of the present catalyst is too small to produce La_2O_3 as a separate phase and is consequently also too small to produce, in the presence of sulfur, enough oxysulfide La_2O_2S compound [17], which would protect the nickel metal from sulfidation. Additionally, the conditions of our experiments may not produce H_2S, which was the only sulfur compound investigated before on lanthana sorbents [17]. Future investigations with a two-zone system (sorbent/catalyst) and different sulfur compounds are warranted.

5. Summary/conclusions

The following summary/conclusion points are drawn from the findings of this work:

1. Ni disperses on pure alumina as a surface $Ni_xAl_2O_{3+x}$ spinel, evident by XRD, XPS, skeletal IR and Vis spectroscopy measurements. This catalyst is slightly less reducible (and less easily conditioned) than previous catalysts containing also some silica (5% SiO_2).
2. La disperses on the alumina in a disordered way. No evidence of lanthanum aluminate formation.
3. The surface $Ni_xAl_2O_{3+x}$ spinel forms also when Ni is deposited on Lanthana on alumina. In the ternary system XPS reveals significant Ni–La interactions.

4. The addition of lanthanum (at 20 wt% La_2O_3) promotes the activity of Ni/Al_2O_3 for ESR and EPSR
5. Fresh unreduced catalysts condition themselves in the feed at temperatures above 973 K
6. Conditioned catalysts give rise to full conversion of reactants in ESR and EPSR at 873 K and above
7. Main by-products when steam reforming activity is still low are ethylene, acetaldehyde and methane, all produced by parallel reactions on different catalyst/support surface sites.
8. Lanthanum reduces the acidity of the support, thus effectively decreasing the dehydration of ethanol to ethylene
9. The sudden start of the steam reforming activity at 873 K corresponds to the temperature onset for the activation of water, to which the support likely participates.
10. Sulfur resistance is not improved because the nickel is exposed in metallic form after pre-reduction at 1023 K, and the lanthana component does not protect the nickel in the present catalyst formulation. It is worth adding a zone of LA upsteam of the NiLA catalyst to examine the use of LA as sorbent of the sulfur species.

Acknowledgements

The financial support by the DOE/BES under Grant # DE-FG02-05ER15730 for the work conducted at Tufts University is gratefully acknowledged. Dr. S. Speakman at MIT's CMSE and Dr. H. Lin at Harvard University's CNS are acknowledged for their assistance with the XRD and XPS work. E.F. acknowledges Università degli Studi di Genova for funding (PRA2013). G.G. acknowledges University of Genova for the support to conduct research at Tufts University.

References

[1] K. Aasberg-Petersen, I. Dybkjær, C.V. Ovesen, N.C. Schjødt, J. Sehested, S.G. Thomsen, J. Nat. Gas Sci. Eng. 3 (2011) 423–459.
[2] J.R. Rostrup-Nielsen, J. Bøgild Hansen, Fuel Cells (2011) 49–71.
[3] T. Sperle, D. Chen, R. Lødeng, A. Holmen, Appl. Catal. A: Gen. 282 (2005) 195–204.
[4] G. Busca, Heterogeneous Catalytic Materials, Elsevier, 2014, 2015, pp.318–321.
[5] S. Qi, X. Yong Wei, Z. Zong, Y. Wang, RSC Adv. 3 (2013) 14219–14232.
[6] G. Busca, Adv. Catal. 57 (2014) 319–404.
[7] J. Sun, Y. Wang, ACS Catal. 4 (2014) 1078–1090.
[8] G. Nahar, V. Dupont, Biofuels 3 (2012) 167–191.
[9] F. Basile, S. Albertazzi, D. Barbera, P. Benito, J. Einvall, J. Brandin, G. Fornasari, F. Trifirò, A. Vaccari, Biomass Bioenergy 35 (2011) S116–S122.
[10] F.L. Chan, A. Tanksale, Renew. Sust. Energy Rev. 38 (2014) 428–438.
[11] E.C. Vagia, A.A. Lemonidou, Appl. Catal. A: Gen. 351 (2008) 111–121.
[12] G. Garbarino, A. Lagazzo, P. Riani, G. Busca, Appl. Catal. B: Environ. 129 (2013) 460–472.
[13] G. Garbarino, E. Finocchio, A. Lagazzo, I. Valsamakis, P. Riani, V. Sanchez Escribano, G. Busca, Appl. Catal. B: Environ. 147 (2014) 813–826.
[14] B. Béguin, E. Garbowski, M. Primet, Appl. Catal. 75 (1991) 119–132.
[15] S. Nathesakawat, R.B. Watson, X.Q. Wang, U.S. Ozkan, J. Mol. Catal. A: Chem. 241 (2005) 133–146.
[16] M.C. Sánchez- Sánchez, R.M. Navarro, J.J.G. Fierro, Catal. Today 129 (2007) 336–345.
[17] K.W. Siew, H.C. Lee, J. Gimbun, C.K. Cheng, Int. J. Hydrogen Energy 39 (2014) 6927–6936.
[18] D.A. Constantinou, M.C. Alvarez-Galvan, J.L.G. Fierro, A.M. Efstathiou, Appl. Catal. B: Environ. 117–118 (2012) 81–95.
[19] I. Valsamakis, M. Flytzani-Stephanopoulos, Appl. Catal. B: Environ. 106 (2011) 255–263.
[20] Pearson Crystal Data: Crystal structure database for inorganic compounds, Release 2009/2012, ASM International, The Material Information Society.
[21] G. Garbarino, A. Romero Perez, E. Finocchio, G. Busca, Cat. Commun. 38 (2013) 67–73.
[22] G. Busca, Catal. Today 226 (2014) 2–13.
[23] G. Busca, V. Lorenzelli, V. Sanchez Escribano, Chem. Mater. 4 (1992) 595–605.
[24] G. Busca, P. Riani, G. Garbarino, G. Ziemacki, L. Gambino, E. Montanari, R. Millini, Appl. Catal. A: Gen. 486 (2014) 176–186.
[25] G. Garbarino, S. Campodonico, A. Romero Perez, M.M. Carnasciali, P. Riani, E. Finocchio, G. Busca, Appl. Catal. A: Gen. 452 (2013) 163–173.
[26] G. Garbarino, I. Valsamakis, P. Riani, G. Busca, Cat. Commun. 51 (2014) 37–41.
[27] A. Tirsoaga, D. Visinescu, B. Jurca, A. Ianculescu, O. Carp, J. Nanopart. Res. 13 (2011) 6397–6408.
[28] G. Busca, Chem. Rev. 110 (2010) 2217–2249.
[29] G. Busca, V. Lorenzelli, Mater. Chem. 7 (1982) 89–126.
[30] C.E. Moffatt, B. Chen, D.M. Wieliczka, M.B. Kruger, Solid State Commun. 116 (2000) 631–636.
[31] Y. Kameshima, A. Yasumori, K. Okada, J. Surf. Sci. Soc. Jpn. 21 (2000) 481–487.
[32] F. El Gabaly, K.F. McCarty, H. Bluhm, A.H. McDaniel, Phys. Chem. Chem. Phys. 15 (2013) 8334–8341.
[33] M. Ferrandon, E. Björnbom, J. Catal. 200 (2001) 148–159.
[34] S. Mickevičius, S. Grebinskij, V. Bondarenka, B. Vengalis, K. Sliuziene, B.A. Orlowski, V. Osinniy, W. Drube, J. Alloy. Compd. 423 (2006) 107–111.
[35] Z. Boukha, L. Fitian, M. López-Haro, M. Mora, J.R. Ruiz, C. Jiménez-Sanchidrián, G. Blanco, J.J. Calvino, G.A. Cifredo, S. Trasobares, S. Bernal, J. Catal. 272 (2010) 121–130.
[36] J. Zheng, X. Ren, Y. Song, X. Ge, React. Kinet. Catal. Lett. 97 (2009) 109–114.
[37] K. Ikkour, D. Sellam, A. Kiennemann, S. Tezkratt, O. Cherifi, Catal. Lett. 132 (2009) 213–217.
[38] G. Ke Zhang, Zhou, J. Li, K. Zhen, T. Cheng, Catal. Lett. 130 (2009) 246–253.
[39] E. Heracleous, A.F. Lee, K. Wilson, A.A. Lemonidou, J. Catal. 231 (2005) 159–171.
[40] K. Polychronopoulou, A.M. Efstathiou, Catal. Today 116 (2006) 341–347.
[41] J.H. Kwak, D. Mei, C.H.F. Peden, R. Rousseau, J. Szanyi, Catal. Lett. 141 (2011) 649.
[42] M.P. Rosynek, R.J. Koprowski, G.N. Dellisante, J. Catal. 122 (1990) 80–94.
[43] P. Riani, G. Garbarino, M.A. Lucchini, F. Canepa, G. Busca, J. Mol. Catal. A: Chem. 383–384 (2014) 10–16.
[44] T.K. Phung, L. Proietti Hernandez, G. Busca, Appl. Catal. A Gen. 489 (2015) 180–187.
[45] B. Manoj, A.G. Kunjomana, Int. J. Electrochem. Sci. 7 (2012) 3127–3134.
[46] S. Helveg, J. Sehested, J.R. Røstrup-Nielsen, Catal. Today 178 (2011) 42–46.
[47] A.N. Fatsikostas, X.E. Verykios, J. Catal. 225 (2004) 439–452.
[48] J.A. Torres, J. Llorca, A. Casanovas, M. Domínguez, J. Salvadò, D. Montané, J. Power Sources 160 (2007) 158–166.
[49] G. Garbarino, V. Sanchez Escribano, E. Finocchio, G. Busca, Appl. Catal. B: Environ. 113–114 (2012) 281–289.
[50] T.K. Phung, A. Lagazzo, M. Á. Rivero Crespo, V. Sánchez Escribano, G. Busca, J. Catal. 311 (2014) 102–113.
[51] P. Riani, G. Garbarino, M.A. Lucchini, F. Canepa, G. Busca, Int. J. Hydrogen Energy 38 (2013) 82–91.
[52] K. Polychronopoulou, C.N. Costa, A.M. Efstathiou, Catal. Today 112 (2006) 89–93.